Published for SISSA by Springer

Received: October 30, 2019
Revised: December 23, 2019
Accepted: January 2, 2020
Published: January 20, 2020

Maximum value of the spin-independent cross section in the 2HDM+a

Tomohiro Abe,[a,b] **Motoko Fujiwara,**[c] **Junji Hisano**[b,c,d] **and Yutaro Shoji**[b]

[a] *Institute for Advanced Research, Nagoya University, Furo-cho Chikusa-ku, Nagoya, 464-8602 Japan*
[b] *Kobayashi-Maskawa Institute for the Origin of Particles and the Universe, Nagoya University, Furo-cho Chikusa-ku, Nagoya, 464-8602 Japan*
[c] *Department of Physics, Nagoya University, Furo-cho Chikusa-ku, Nagoya, 464-8602 Japan*
[d] *Kavli IPMU (WPI), UTIAS, University of Tokyo, Kashiwa, 277-8584 Japan*

E-mail: abetomo@kmi.nagoya-u.ac.jp, motoko@eken.phys.nagoya-u.ac.jp, hisano@eken.phys.nagoya-u.ac.jp, yshoji@kmi.nagoya-u.ac.jp

Abstract: We investigate the maximum value of the spin-independent cross section ($\sigma_{\rm SI}$) in a dark matter (DM) model called the two-Higgs doublet model + a (2HDM+a). This model can explain the measured value of the DM energy density by the freeze-out mechanism. Also, $\sigma_{\rm SI}$ is suppressed by the momentum transfer at the tree level, and loop diagrams give the leading contribution to it. The model prediction of $\sigma_{\rm SI}$ highly depends on values of c_1 and c_2 that are the quartic couplings between the gauge singlet CP-odd state (a_0) and Higgs doublet fields (H_1 and H_2), $c_1 a_0^2 H_1^\dagger H_1$ and $c_2 a_0^2 H_2^\dagger H_2$. We discuss the upper and lower bounds on c_1 and c_2 by studying the stability of the electroweak vacuum, the condition for the potential bounded from the below, and the perturbative unitarity. We find that the condition for the stability of the electroweak vacuum gives upper bounds on c_1 and c_2. The condition for the potential to be bounded from below gives lower bounds on c_1 and c_2. It also constrains the mixing angle between the two CP-odd states. The perturbative unitarity bound gives the upper bound on the Yukawa coupling between the dark matter and a_0 and the quartic coupling of a_0. Under these theoretical constraints, we find that the maximum value of the $\sigma_{\rm SI}$ is $\sim 5 \times 10^{-47}\,{\rm cm}^2$ for $m_A = 600\,{\rm GeV}$, and the LZ and XENONnT experiments can see the DM signal predicted in this model near future.

Keywords: Beyond Standard Model, Higgs Physics

ArXiv ePrint: 1910.09771

https://doi.org/10.1007/JHEP01(2020)114

Contents

JHEP01(2020)114

1 Introduction

One of the great achievements in Cosmology is the precise determination of the energy density of the dark matter (DM) by the Planck collaboration, $\Omega h^2 = 0.120 \pm 0.001$ [1]. The measured value is explained successfully by DM models that use the freeze-out mechanism [2], which have been widely studied for a long time. Those models generally predict non-zero DM-nucleon scattering cross section and have been searched by the direct detection experiments, such as the Xenon1T experiment [3]. However, no significant signals have been observed until now, and the null results set upper bound on the DM-nucleon scattering cross section. The latest result by the Xenon1T experiment gives a severe constraint on DM models.

If a DM particle is a gauge singlet fermion, χ, and couples to a scalar mediator, a_0, with pseudo-scalar type interaction, $\bar{\chi} i \gamma_5 \chi a_0$, then it is possible to avoid this strong constraint from the Xenon1T experiment while keeping the success of the freeze-out mechanism [4, 5].

The two-Higgs doublet model + a (2HDM+a) [6] is one of the models that realize this idea.[1] In addition to the introduction of the DM and the mediator, the Higgs sector is extended into the two-Higgs doublet model. The CP invariance is assumed in the dark sector and the scalar sector. Then, the dark sector and the visible sector can interact through the mixing between a_0 and the CP-odd scalar (A_0) in the two-Higgs doublet sector. The model predicts rich phenomenology [10–17], and it is summarized in ref. [18].

The 2HDM+a predicts non-zero spin-independent DM-nucleon scattering cross section ($\sigma_{\rm SI}$) at loop level [6, 14, 16, 17, 19]. In particular, it was shown that if c_2, which is a quartic coupling between a_0 and a Higgs doublet field H_2, is large enough, the model can be tested at the forthcoming direct detection experiments [19]. However, such a large coupling causes theoretical problems. If the coupling takes large negative value, the potential can be unbounded from the below. If the coupling is very large, it hits a Landau pole near the electroweak scale and the model loses predictability.

In this paper, we study the constraint on the scalar potential from the boundedness of the scalar potential, the stability of the electroweak vacuum, and perturbative unitarity. Using these constraints, we investigate the upper and the lower bounds on the scalar quartic couplings, and discuss the maximum value of $\sigma_{\rm SI}$. We show that the maximum value of $\sigma_{\rm SI}$ is below the current constraint from the Xenon1T experiment and above the prospect of the LZ experiment [20] and the XENONnT experiment [21].

The rest of the paper is organized as follows. In section 2, we briefly describe the 2HDM+a. In section 3, we investigate theoretical constraints on the model parameters. Conditions for the electroweak vacuum as the global minimum of the scalar potential, for the potential to be bounded from below, and for perturbative unitarity for the quartic couplings in the scalar potential are discussed. These conditions are used to find the upper and the lower bounds on c_1 and c_2 and the upper bound on the mixing angle between the two CP-odd states. In section 4, we scan the model parameter space and find the maximum value of $\sigma_{\rm SI}$ under the constraint discussed in section 3. Section 5 is devoted to our conclusion.

2 Model

The model contains a gauge singlet Majorana fermion χ as a DM candidate and a CP-odd gauge singlet scalar a_0 as a mediator. The standard model (SM) Higgs sector is extended into the two-Higgs doublet model. We assume CP invariance both in the dark sector and in the scalar sector. This assumption guarantees that the Yukawa interaction between χ and a_0 is always pseudo-scalar interaction. The Lagrangian is given by

$$\begin{aligned}\mathcal{L} = &\frac{1}{2}\bar{\chi}\left(i\partial\!\!\!/ - m_{\rm DM}\right)\chi - \frac{g_\chi}{2}\bar{\chi}i\gamma^5\chi a_0 \\ &+ \frac{1}{2}\partial_\mu a_0 \partial^\mu a_0 + D_\mu H_1^\dagger D^\mu H_1 + D_\mu H_2^\dagger D^\mu H_2 - V_{\rm scalar} \\ &+ (\text{terms with the SM fermions and gauge bosons}),\end{aligned} \tag{2.1}$$

[1] Other realizations are discussed in, for example, refs. [7, 8]. Another mechanism to avoid the constraint from direct detection experiments is studied in ref. [9].

JHEP01(2020)114

where

$$
\begin{aligned}
V_{\rm scalar} &= m_1^2 H_1^\dagger H_1 + m_2^2 H_2^\dagger H_2 - m_3^2 \left(H_1^\dagger H_2 + (\text{h.c.}) \right) \\
&+ \frac{1}{2}\lambda_1 (H_1^\dagger H_1)^2 + \frac{1}{2}\lambda_2 (H_2^\dagger H_2)^2 + \lambda_3 (H_1^\dagger H_1)(H_2^\dagger H_2) + \lambda_4 (H_1^\dagger H_2)(H_2^\dagger H_1) \\
&+ \frac{1}{2}\lambda_5 \left((H_1^\dagger H_2)^2 + (\text{h.c.}) \right) \\
&+ \frac{1}{2} m_{a_0}^2 a_0^2 + \frac{\lambda_a}{4} a_0^4 + \kappa \left(i a_0 H_1^\dagger H_2 + (\text{h.c.}) \right) + c_1 a_0^2 H_1^\dagger H_1 + c_2 a_0^2 H_2^\dagger H_2 .
\end{aligned} \tag{2.2}
$$

Since we assume the CP invariant scalar potential, all the couplings in the potential are real. In this paper, we assume that the thermal relic abundance of χ explains the measured value of the DM energy density [1], and g_χ is fixed to realized it for a given parameter set by the freeze-out mechanism.

We impose the condition that the potential has the electroweak vacuum,

$$
\langle a_0 \rangle = 0, \ \langle H_1 \rangle = \begin{pmatrix} 0 \\ \frac{1}{\sqrt{2}} v_1 \end{pmatrix}, \ \langle H_2 \rangle = \begin{pmatrix} 0 \\ \frac{1}{\sqrt{2}} v_2 \end{pmatrix}. \tag{2.3}
$$

This electroweak vacuum is realized if m_1^2 and m_2^2 satisfy the following relations.

$$
m_1^2 = -\frac{v_1^2 \lambda_1 + v_2^2 \lambda_{345}}{2} + m_3^2 \frac{v_2}{v_1}, \tag{2.4}
$$

$$
m_2^2 = -\frac{v_2^2 \lambda_2 + v_1^2 \lambda_{345}}{2} + m_3^2 \frac{v_1}{v_2}, \tag{2.5}
$$

where $\lambda_{345} = \lambda_3 + \lambda_4 + \lambda_5$. In the following, we assume m_1^2 and m_2^2 always satisfy these relations. It is also important that a_0 does not develop vacuum expectation value. Otherwise, the scalar-type Yukawa interaction is induced in the dark sector due to the scalar and pseudo-scalar mixing, and the model is strongly constrained from the direct detection experiments.

After the electroweak symmetry breaking, there are two CP-even scalars (h and H), two CP-odd scalars (a and A), a pair of charged scalars ($H^\pm$), and three would-be Nambu-Goldstone bosons that are eaten by $W^\pm$ and Z. The physical masses for h, H, a, A, and $H^\pm$ are denoted to m_h, m_H, m_a, m_A, and $m_{H^\pm}$, respectively. The two CP-even scalars are mixtures of the CP-even neutral components in H_1 and H_2, and its mixing angle is denoted by α. Similarly, the two CP-odd scalars are mixtures of the CP-odd neutral components in H_1 and H_2 and also a_0. Its mixing angle is denoted by θ.

We introduce the following notations for later convenience,

$$
t_\beta = \tan\beta = \frac{v_2}{v_1}, \quad s_\beta = \sin\beta, \quad c_\beta = \cos\beta, \tag{2.6}
$$

$$
v = \sqrt{v_1^2 + v_2^2}, \tag{2.7}
$$

$$
M^2 = \frac{v_1^2 + v_2^2}{v_1 v_2} m_3^2. \tag{2.8}
$$

JHEP01(2020)114

Let us comment on the types of the Yukawa interaction. The model is classified into four types based on the Yukawa interaction between the two-Higgs doublet fields and the SM fermions, as in the two-Higgs doublet model with softly broken Z_2 symmetry [22–24]. In the following analysis, we choose the type-I Yukawa interaction where H_2 couples to the SM fermions but H_1 does not. The following discussion is independent from the types of the Yukawa interaction because the type dependence is negligible for large $\sigma_{\rm SI}$ region of the parameter space as we showed in our previous work [19], and the purpose of this paper is to find the maximum value of $\sigma_{\rm SI}$ for a given parameter set.

We can express λ_i $(i = 1, 2, 3, 4, 5)$, κ, and $m_{a_0}^2$ by the mixing angles and mass eigenvalues. In the followings, we take the mixing angle in the CP-even scalars as $\alpha = \beta - \pi/2$. This choice predicts the same hWW and the hZZ couplings as in the SM. We also take $M = m_H = m_A = m_{H^\pm}$. This choice of the mass parameters enhances the custodial symmetry in the scalar potential, and thus the constraints from the electroweak precision measurements are automatically satisfied. With these parameter choices, the parameters of the scalar potential are given by

$$\lambda_1 = \lambda_2 = \lambda_3 = \frac{m_h^2}{v^2}, \tag{2.9}$$

$$\lambda_4 = -\lambda_5 = -\frac{m_A^2 - m_a^2}{v^2} s_\theta^2, \tag{2.10}$$

$$\kappa = -\frac{m_A^2 - m_a^2}{2v} \sin 2\theta, \tag{2.11}$$

$$m_{a_0}^2 = m_a^2 c_\theta^2 + m_A^2 s_\theta^2 - \frac{c_1 + c_2 t_\beta^2}{1 + t_\beta^2} v^2. \tag{2.12}$$

As can be seen, $|\lambda_{1,2,3}| < 1$. We can also show that $|\lambda_{4,5}| < 1$ with a condition for the boundedness of the scalar potential (eq. (3.17)) discussed in the next section.

3 Theoretical constraints on the scalar potential

In this section, we discuss the condition for the electroweak vacuum as the global minimum of the scalar potential, the conditions for the potential to be bounded from below, and the perturbative unitarity for the quartic couplings in the scalar potential. These constraints are used to find the upper and the lower bounds on c_1, c_2, and θ.

3.1 Vacuum structure

Vacua other than the electroweak vacuum can exist depending on the given parameter sets. We study the vacuum structure at the tree level and impose the condition that the electroweak vacuum should be the global minimum. It is not necessary for the electroweak vacuum to be the global minimum if its lifetime is much longer than the age of our Universe. However, the lifetime is much shorter than the age of the Universe in most of the parameter space.[2] Therefore, we adopt the condition to be the global minimum in the current analysis.

[2]The lifetime is estimated by using `SimpleBounce` [25].

JHEP01(2020)114

3.1.1 $\langle H_1 \rangle = \langle H_2 \rangle = 0$

In this case, the stationary condition for the scalar potential is given by

$$a_0 \left(m_{a_0}^2 + \lambda_a a_0^2 \right) = 0. \tag{3.1}$$

If $m_{a_0}^2 < 0$, we have vacua where a_0 develops the vacuum expectation value. The sign of $m_{a_0}^2$ depends on the values of c_1, c_2, and t_β as in eq. (2.12). Since we impose the condition that the electroweak vacuum should be the global minimum, such vacua should not be deeper than the electroweak vacuum.

At the vacuum with $\langle a_0 \rangle \neq 0$, the potential energy is given by

$$V_{\text{min.}}|_{\langle H_1 \rangle = \langle H_2 \rangle = 0, \langle a_0 \rangle \neq 0} = -\frac{m_{a_0}^4}{4\lambda_a}. \tag{3.2}$$

This should be larger than the potential energy at the electroweak vacuum,

$$V_{\text{min.}}|_{\langle H_1 \rangle \neq 0, \langle H_2 \rangle \neq 0, \langle a_0 \rangle = 0} = -\frac{1}{8} \left(m_h^2 s_{\beta-\alpha}^2 + m_H^2 c_{\beta-\alpha}^2 + \frac{4(m_{H^\pm}^2 - m_H^2) t_\beta^2}{(1+t_\beta^2)^2} \right) v^2. \tag{3.3}$$

Therefore, we obtain the following condition for $m_{a_0}^2 < 0$,

$$\lambda_a \left(m_h^2 s_{\beta-\alpha}^2 + m_H^2 c_{\beta-\alpha}^2 + \frac{4(m_{H^\pm}^2 - m_H^2) t_\beta^2}{(1+t_\beta^2)^2} \right) > \frac{2 m_{a_0}^4}{v^2}. \tag{3.4}$$

From eqs. (2.12) and (3.4), for $\sin(\beta - \alpha) = 1$ and $M = m_H = m_A = m_{H^\pm}$, we find

$$\frac{c_1 + c_2 t_\beta^2}{1 + t_\beta^2} < \sqrt{\frac{\lambda_a m_h^2}{2v^2}} + \frac{m_a^2 c_\theta^2 + m_A^2 s_\theta^2}{v^2}. \tag{3.5}$$

As a result, we obtain the upper bound on c_1 or c_2 for a given parameter sets.

3.1.2 One of $\langle H_1 \rangle$ and $\langle H_2 \rangle$ is zero

We investigate $\langle H_1 \rangle = 0$ and $\langle H_2 \rangle \neq 0$. Without lose of the generality, we can parametrize the vacuum as

$$\langle H_2 \rangle = \begin{pmatrix} 0 \\ \frac{1}{\sqrt{2}} \sigma_2 \end{pmatrix}. \tag{3.6}$$

A stationary condition of this vacuum is given by

$$0 = -m_3^2 \sigma_2. \tag{3.7}$$

This condition is obtained in both $\langle a_0 \rangle = 0$ and $\langle a_0 \rangle \neq 0$ cases. Since $m_3^2 \neq 0$, see eq. (2.8), this condition implies $\sigma_2 = 0$. This is contradict to $\langle H_2 \rangle \neq 0$. Therefore, we do not have vacua that satisfy $\langle H_1 \rangle = 0$ and $\langle H_2 \rangle \neq 0$.

In the same manner, we can show that we do not have vacua that satisfy $\langle H_1 \rangle \neq 0$ and $\langle H_2 \rangle = 0$.

JHEP01(2020)114

3.1.3 $\langle H_1 \rangle \neq 0$ and $\langle H_2 \rangle \neq 0$

We simplify the analysis as much as possible by using the gauge invariance in the potential. Without lose of the generality, we can parametrize the Higgs fields as

$$\langle H_1 \rangle = \begin{pmatrix} 0 \\ \frac{1}{\sqrt{2}}\sigma_1 \end{pmatrix}, \quad \langle H_2 \rangle = \begin{pmatrix} \pi_2^+ \\ \frac{1}{\sqrt{2}}(\sigma_2 + i\pi_2^0) \end{pmatrix}, \tag{3.8}$$

where σ_1 is positive and σ_2, π_2^0, and π_2^+ are real numbers. In this case, since the analysis is complicated, we rely on numerical analysis.

3.2 Conditions for the potential to be bounded from below

The potential should be bounded from below. In other words, the potential should be positive for the region where the field values are extremely large. We find the following seven conditions for the boundedness of the scalar potential.

$$\lambda_1 > 0, \tag{3.9}$$

$$\lambda_2 > 0, \tag{3.10}$$

$$\lambda_a > 0, \tag{3.11}$$

$$\sqrt{\lambda_1 \lambda_2} + \tilde{\lambda}_3 > 0, \tag{3.12}$$

$$\sqrt{\frac{\lambda_1 \lambda_a}{2}} + c_1 > 0, \tag{3.13}$$

$$\sqrt{\frac{\lambda_2 \lambda_a}{2}} + c_2 > 0, \tag{3.14}$$

$$\begin{cases} \sqrt{\lambda_1} c_2 + \sqrt{\lambda_2} c_1 \geq 0, \\ \text{or} \\ \sqrt{\lambda_1} c_2 + \sqrt{\lambda_2} c_1 < 0 \text{ and } \frac{\lambda_a \tilde{\lambda}_3}{2} - c_1 c_2 + \sqrt{\left(\frac{\lambda_a \lambda_1}{2} - c_1^2\right)\left(\frac{\lambda_a \lambda_2}{2} - c_2^2\right)} > 0. \end{cases} \tag{3.15}$$

where

$$\tilde{\lambda}_3 = \lambda_3 + \min(0, \lambda_4 - |\lambda_5|). \tag{3.16}$$

The derivation is given in appendix A.[3] As can be seen, eqs. (3.13), (3.14), and (3.15) give the lower bounds on c_1 and c_2.

We find that eq. (3.12) gives a constraint on θ. For $s_{\beta-\alpha} = 1$ and $M = m_H = m_A = m_{H^\pm}$, using eqs. (2.9) and (2.10), we can simplify eq. (3.12) as

$$|\sin\theta| < \frac{m_h}{\sqrt{m_A^2 - m_a^2}}. \tag{3.17}$$

[3]The scalar potential discussed in ref. [26] is the same as in this paper, but they find that the second condition in eq. (3.15) should be applied for c_1 or $c_2 < 0$. The condition given in ref. [28], which was derived from the result given in ref. [29], is consistent with our result. The condition given in ref. [30] is different from ours.

JHEP01(2020)114

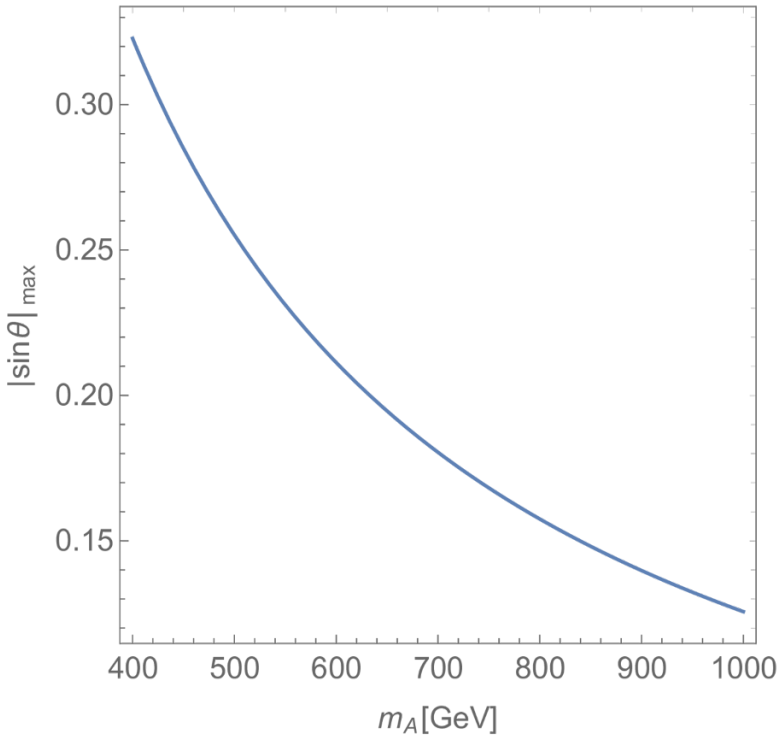

Figure 1. The upper bound on θ obtained from eq. (3.17). Here we take $s_{\beta-\alpha} = 1$, $m_a = 100\,\text{GeV}$, and $m_H = m_{H^\pm} = m_A$.

The constraint on $|\sin\theta|$ by using this result for $m_a = 100\,\text{GeV}$ is shown in figure 1. We find that $|\sin\theta| \lesssim 0.21$ for $m_A = 600\,\text{GeV}$, and $|\sin\theta| \lesssim 0.13$ for $m_A = 1\,\text{TeV}$.

For $s_{\beta-\alpha} = 1$ and $M = m_H = m_A = m_{H^\pm}$, we can also simplify other conditions with physical observables as follows.

$$\sqrt{\frac{\lambda_a}{2}}\frac{m_h}{v} + c_1 > 0, \tag{3.18}$$

$$\sqrt{\frac{\lambda_a}{2}}\frac{m_h}{v} + c_2 > 0, \tag{3.19}$$

$$\begin{cases} c_1 + c_2 \geq 0, \\ \text{or} \\ c_1 + c_2 < 0 \text{ and } \frac{\lambda_a}{2}\left(\frac{m_h^2}{v^2} - \frac{2(m_A^2 - m_a^2)}{v^2}s_\theta^2\right) - c_1 c_2 + \sqrt{\left(\frac{\lambda_a m_h^2}{2v^2} - c_1^2\right)\left(\frac{\lambda_a m_h^2}{2v^2} - c_2^2\right)} > 0. \end{cases} \tag{3.20}$$

3.3 Perturbative unitarity

Constraints on scalar quartic couplings are often derived from the perturbative unitarity of two scalars to two scalars scattering processes. There are nine scalars in the model. Therefore, the two to two scattering matrix that only includes scalars is a 45×45 matrix. Since we consider the high energy limit and ignore the gauge couplings, the scattering

JHEP01(2020)114

processes are s-wave. In the following analysis, the Yukawa coupling, g_χ, often takes $\mathcal{O}(1)$ value, and thus we also include DM two body initial and final states in the matrix. The DM particle takes two helicity states. In the high energy limit, we find that two DM particles into two DM particles processes are s-wave, and two DM particles into two scalars processes are p-wave. The former processes give stronger bound on g_χ. We impose absolute values of each eigenvalue of the matrix are less than 8π and find that [27, 28]

$$|c_1| < 4\pi, \tag{3.21}$$

$$|c_2| < 4\pi, \tag{3.22}$$

$$|\lambda_3 \pm \lambda_4| < 8\pi, \tag{3.23}$$

$$\left|\frac{1}{2}\left(\lambda_1+\lambda_2 \pm \sqrt{(\lambda_1-\lambda_2)^2+4\lambda_4^2}\right)\right| < 8\pi, \tag{3.24}$$

$$\left|\frac{1}{2}\left(\lambda_1+\lambda_2 \pm \sqrt{(\lambda_1-\lambda_2)^2+4\lambda_5^2}\right)\right| < 8\pi, \tag{3.25}$$

$$|\lambda_3+2\lambda_4 \pm 3\lambda_5| < 8\pi, \tag{3.26}$$

$$|\lambda_3 \pm \lambda_5| < 8\pi, \tag{3.27}$$

$$g_\chi^2 < 4\pi, \tag{3.28}$$

$$|x_i| < 8\pi \ (i=1,2,3), \tag{3.29}$$

where x_i are solutions of the following equation,

$$\begin{aligned} 0 = {} & x^3 - 3\left(\lambda_a+\lambda_1+\lambda_2\right)x^2 \\ & + \left(-4c_1^2-4c_2^2-4\lambda_3^2-4\lambda_3\lambda_4-\lambda_4^2+9\lambda_1\lambda_2+9\lambda_1\lambda_a+9\lambda_2\lambda_a\right)x \\ & + 12c_2^2\lambda_1+12c_1^2\lambda_2-16c_1c_2\lambda_3-8c_1c_2\lambda_4+\left(-27\lambda_1\lambda_2+12\lambda_3^2+12\lambda_3\lambda_4+3\lambda_4^2\right)\lambda_a. \end{aligned} \tag{3.30}$$

For $|\lambda_i| \ll 1$ $(i=1,2,3,4,5)$, eq. (3.29) is simplified as

$$\frac{1}{2}\left(3\lambda_a+\sqrt{16c_1^2+16c_2^2+9\lambda_a^2}\right) < 8\pi, \tag{3.31}$$

or

$$\lambda_a < \frac{8\pi}{3}\left(1-\frac{c_1^2+c_2^2}{16\pi^2}\right). \tag{3.32}$$

Since $\lambda_a > 0$, this inequality implies that

$$\sqrt{c_1^2+c_2^2} < 4\pi. \tag{3.33}$$

This gives stronger constraint on c_1 and c_2 than eqs. (3.21) and (3.22).

For $s_{\beta-\alpha}=1$ and $M=m_H=m_A=m_{H^\pm}$, using eqs. (2.9) and (2.10), we can simplify the perturbative unitarity conditions $\lambda_{1,2,3,4,5}$ (eqs. (3.23)–(3.27)) and express them with masses of the scalars as follows.

$$|m_h^2 \pm (m_A^2-m_a^2)s_\theta^2| < 8\pi v^2, \tag{3.34}$$

$$|m_h^2 - 5(m_A^2-m_a^2)s_\theta^2| < 8\pi v^2. \tag{3.35}$$

JHEP01(2020)114

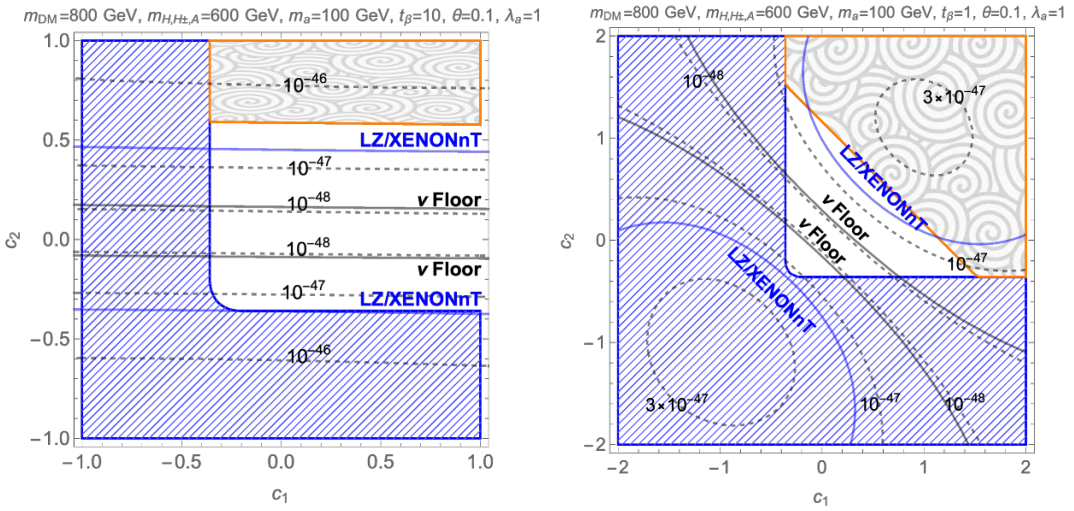

Figure 2. The contours for $\sigma_{\rm SI}$ [cm^2] for $m_{\rm DM} = 800\,\text{GeV}$ are shown by the dashed curves. The blue solid lines show the LZ and XENONnT prospects [20, 21], In both panels, we take $m_H = m_{H^\pm} = m_A = 600\,\text{GeV}$, $m_a = 100\,\text{GeV}$, $\theta = 0.1$, and $\lambda_a = 1$. The left (right) panel is for $t_\beta = 10$ (1). The region between two black solid lines is below the neutrino floor [31]. The global minimum does not break the electroweak symmetry in the region surrounded by the orange line and filled with the spirals pattern. In the blue shaded region with hatching, the scalar potential is unbounded from the below.

4 Spin-independent scattering cross section

We discuss the maximum value of $\sigma_{\rm SI}$ under the constraints discussed in section 3. We find upper bounds on c_1 and c_2 from the stability of the electroweak vacuum, and lower bounds from the boundedness of the scalar potential. Since $g_\chi \sim \mathcal{O}(1)$ in the large $\sigma_{\rm SI}$ regime [19], the perturbative unitarity also gives relevant constraint in the parameter space.

The left panel in figure 2 shows that the contours of $\sigma_{\rm SI}$ for $m_{\rm DM} = 800\,\text{GeV}$ with the conditions discussed in sections 3.1 and 3.2. The other parameters except λ_a are the same as one used in figure 8 in ref. [19], namely $m_H = m_{H^\pm} = m_A = 600\,\text{GeV}$, $m_a = 100\,\text{GeV}$, $t_\beta = 10$, $\theta = 0.1$, and $\lambda_a = 1$. It is clearly shown that $\sigma_{\rm SI}$ is larger in the larger $|c_2|$ region as discussed in ref. [19]. It is also shown that there is an upper bound on $\sigma_{\rm SI}$ from the condition discussed in section 3.1. A large positive c_2 predicts that the electroweak vacuum is not the global minimum. This is because such a large positive c_2 makes $m_{a_0}^2$ negatively large as can be seen from eq. (2.12), and thus eq. (3.5) is not satisfied. A large negative c_2 does not satisfy eqs. (3.13)–(3.15) and makes the potential unbounded from the below. These theoretical constraints on the scalar potential give the upper and lower bounds on c_2. Consequently, $\sigma_{\rm SI}$ cannot be arbitrary large. The right panel in figure 2 is a similar to the left panel but with a smaller value of t_β. In this case, there are upper bounds both on c_1 and c_2.

From figure 2, we find a correlation between $\sigma_{\rm SI}$ and the condition of the stability of the electroweak vacuum. The contour of $\sigma_{\rm SI}$ and the boundary of the constraint of the stability of the electroweak vacuum (the edge of the orange shaded region) are almost parallel to

JHEP01(2020)114

each other. We can understand this correlation as follows. For $s_{\beta-\alpha} = 1$ and $m_H = m_{H^\pm}$, the condition to avoid $\langle a_0 \rangle \neq 0$ vacuum given in eq. (3.4) is simplified as

$$\lambda_a > \frac{2m_{a_0}^4}{m_h^2 v^2} \quad (\text{for } m_{a_0}^2 < 0). \tag{4.1}$$

As discussed in ref. [19], both $\sigma_{\rm SI}$ and $\langle \sigma v \rangle$ depend on the a–a–h coupling, g_{aah}, that is given by

$$g_{aah} = s_\theta^2 \left(\frac{2m_a^2 + m_h^2 - 2m_A^2}{v} \right) + 2v c_\theta^2 \frac{c_1 + c_2 t_\beta^2}{1 + t_\beta^2} \tag{4.2}$$

$$= \frac{2(m_a^2 - m_{a_0}^2)}{v} + \mathcal{O}(\theta^2), \tag{4.3}$$

for $s_{\beta-\alpha} = 1$ and $m_H = m_{H^\pm} = m_A$. Combining these two equations, we find

$$\lambda_a > \frac{2v^2}{m_h^2} \left(\frac{m_a^2}{v^2} - \frac{g_{aah}}{2v} \right)^2 + \mathcal{O}\left(\theta^2\right). \tag{4.4}$$

This condition is not satisfied with the large g_{aah}, and thus the large g_{aah} induces the $\langle a_0 \rangle \neq 0$ vacuum. On the other hand, the large g_{aah} is necessary to obtain the larger $\sigma_{\rm SI}$. Therefore, there is a correlation between $\sigma_{\rm SI}$ and the condition of the stability of the electroweak vacuum.

We can also see from figure 2 that the maximum value of $\sigma_{\rm SI}$ is near the boundary of the stability of the electroweak vacuum. For the purpose of finding maximum value of $\sigma_{\rm SI}$, we need to find the maximum value of g_{aah} that satisfies eq. (4.4). The c_1 and c_2 dependent part of g_{aah}, which is the second term in eq. (4.2), depends on t_β. This t_β dependence vanishes for $c_1 = c_2$. We take $c_1 = c_2$ and $t_\beta = 10$ in the following analysis, but the following results are insensitive to the choice of t_β.

The larger λ_a allows us to take larger g_{aah} while keeping $\langle a_0 \rangle = 0$, which can be seen from eq. (4.4). On the other hand, the larger λ_a implies the breakdown of perturbative calculation at a higher energy scale. In our analysis, g_χ is typically $\mathcal{O}(1)$ to obtain the measured value of the DM energy density, and it also implies the breakdown of perturbative calculation at a higher energy scale. We calculate the running of the couplings at the 1-loop level and estimate the cutoff scale Λ as the highest scale that satisfies eqs. (3.11), (3.28), and (3.32). In the calculation, we assume that the input parameters are given at $\mu = m_A$. The beta-functions of the couplings we used are given in appendix B. The smaller λ_a at $\mu = m_A$ becomes negative at higher scale because a_0 couple to the fermionic DM that gives a negative contribution to the beta function of λ_a. On the other hand, the beta function is proportional to λ_a^2 and positive for the larger λ_a. The cutoff scale gives the upper and the lower bounds on λ_a at $\mu = m_A$.

Figure 3 shows the contours of $\sigma_{\rm SI}$ in λ_a–c_2 planes. It is shown that the larger λ_a at $\mu = m_A$ keeps its value positive at any higher scale. We find that it is easy to make the cutoff scale higher than $\mathcal{O}(100)$ TeV by choosing $\lambda_a \simeq 1.5$. Thus we can expect that unknown UV physics does not modify our results for $\lambda_a \simeq 1.5$. We also find that $\sigma_{\rm SI}$ is maximized

JHEP01(2020)114

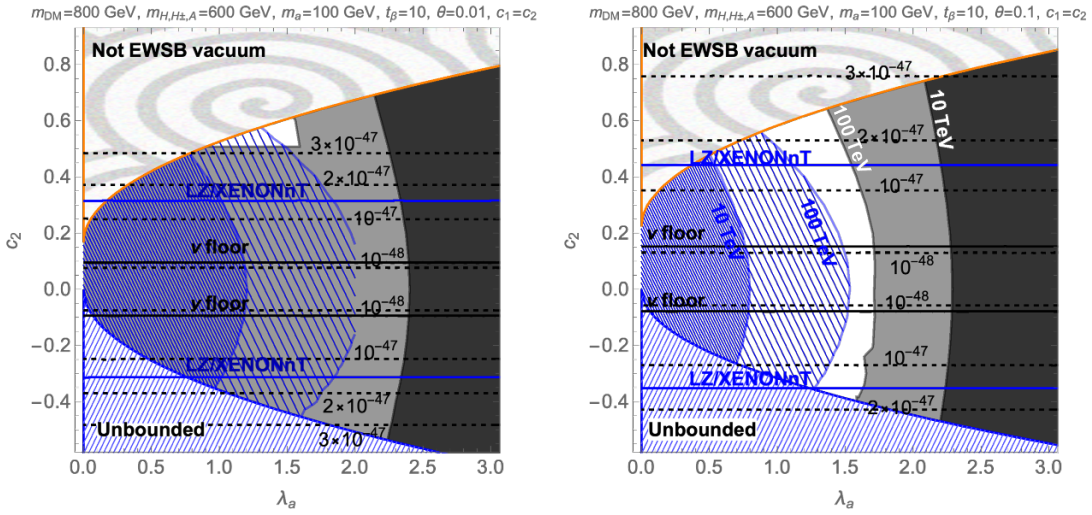

Figure 3. The contours for $\sigma_{\rm SI}$ [cm^2] for $m_{\rm DM} = 800\,$GeV are shown by the dashed curves. In the left (right) panel, $\theta = 0.01$ (0.1). In the thin (dense) blue-hatching region (\\\\), $\lambda_a(\Lambda)$ becomes negative at $\Lambda < 100$ (10) TeV. In the lighter (darker) black region, eq. (3.28) or (3.32) is violated at $\Lambda < 100$ (10) TeV. The other color notation is the same as in figure 2.

along the boundary of the orange shaded region where the electroweak symmetry is not broken. For $c_1 = c_2$, eq. (3.5) is simplified as

$$c_2 < \sqrt{\frac{\lambda_a m_h^2}{2v^2} + \frac{m_a^2 c_\theta^2 + m_A^2 s_\theta^2}{v^2}} \equiv c_*. \tag{4.5}$$

In the following analysis, we choose $c_1 = c_2 = 0.99 c_*$ for given parameter sets. This choice of c_1 and c_2 maximizes $\sigma_{\rm SI}$.

Figure 4 shows the contours of $\sigma_{\rm SI}$ in λ_a–θ plane. We find that $\sigma_{\rm SI}$ is larger in the smaller θ regime. This is because the smaller θ requires larger g_χ to obtain the measured value of the DM energy density. The left and right panels are for $m_A = 600\,$GeV and 1 TeV, respectively. We find that $\sigma_{\rm SI}$ is almost independent from $m_{H,H^\pm,A}$ for $\theta < 0.01$. This is because the heavier scalars almost decouple both from the DM annihilation processes and from the loop contributions to $\sigma_{\rm SI}$. The cutoff scales are the only difference if we change m_A; a larger m_A predicts higher cutoff scales. In the following analysis, we take $\theta = 0.001$. With this choice, $\sigma_{\rm SI}$ is maximized and is independent from m_A. We also take $m_A = 600\,$GeV in the following, which gives us a conservative bound from the RGE analysis.

Figure 5 shows the contours of $\sigma_{\rm SI}$ in λ_a–$m_{\rm DM}$ plane. We take $m_a = 100$, 200, 250, and 280 GeV in each panel. We find that the maximum value of $\sigma_{\rm SI}$ is almost independent of the choice of m_a, $\sigma_{\rm SI} \lesssim 5 \times 10^{-47}\,$cm^2. This value is larger than the prospects of the LZ and XENONnT experiments. Therefore, we have a chance to see the DM direct detection signal near future. The constraint from the perturbative unitarity with the running couplings gives a stronger bound for the larger m_a due to the following reason. As can be seen from eq. (4.5), c_* and hence c_1 and c_2 become larger for the larger m_a. The larger c_1 and c_2 make the beta function of λ_a larger. Therefore, the constraint from the perturbative

JHEP01(2020)114

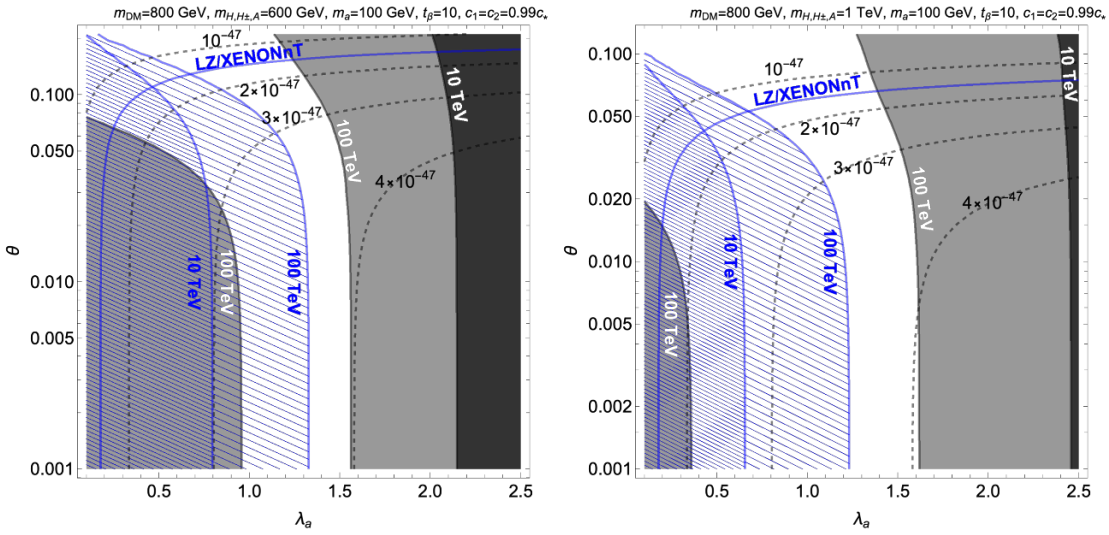

Figure 4. The contours for $\sigma_{\rm SI}$ [cm^2] in λ_a–θ plane. The left (right) panel is for $m_A = 600$ (1000) GeV. The color notation is the same in figure 3.

unitarity with the running couplings becomes severer for larger values of m_a. It is also shown that $\sigma_{\rm SI}$ becomes large for the large $m_{\rm DM}$ regime. This is because larger values of $m_{\rm DM}$ requires larger values of g_χ to obtain the right amount of the relic abundance. On the other hand, larger values of g_χ implies that the Landau pole arises at a lower scale because g_χ is asymptotic non-free. This gives an upper bound on $m_{\rm DM}$ as shown in the figure.

5 Conclusion

The 2HDM+a is a DM model that can explain the measured value of the DM energy density by the freeze-out mechanism and can avoid the constraint from the Xenon1T experiment. The leading order contribution to $\sigma_{\rm SI}$ is given at the loop level, and $\sigma_{\rm SI}$ can be large enough for the model to be tested by the forthcoming direct detection experiments.

In this paper, we have investigated the maximum value of $\sigma_{\rm SI}$ under theoretical constraints. We take into account the stability of the electroweak vacuum, the condition for the potential bounded from the below, and the perturbative unitarity of two to two scattering processes. As shown in figure 2, large $|c_1|$ and $|c_2|$ make $\sigma_{\rm SI}$ larger. However, the condition for the stability of the electroweak vacuum gives upper bounds on c_1 and c_2, and the potential boundedness condition gives lower bounds on them. As a result, there exists the maximum value of $\sigma_{\rm SI}$ for a given parameter set. It is also shown that $\sigma_{\rm SI}$ is maximized for $c_1 = c_2 = c_*$, where c_* is the maximum values of c_1 and c_2 to keep the electroweak vacuum as the global minimum of the scalar potential. With this choice, the result is insensitive to t_β. We found that a smaller θ makes $\sigma_{\rm SI}$ larger, as shown in figure 4. For the small θ regime, $\sigma_{\rm SI}$ is almost independent of $m_{H,H^\pm,A}$. Finally, in figure 5, we found that $\sigma_{\rm SI}$ can be larger than the prospects of the LZ and XENONnT experiments for $m_{\rm DM} \gtrsim 600\,{\rm GeV}$. We also found that the perturbative unitarity gives an upper bound on m_χ. The maximum value of the $\sigma_{\rm SI}$ is $\sim 5\times10^{-47}\,{\rm cm}^2$ for $m_A = 600\,{\rm GeV}$ where the cutoff scale of this model

JHEP01(2020)114

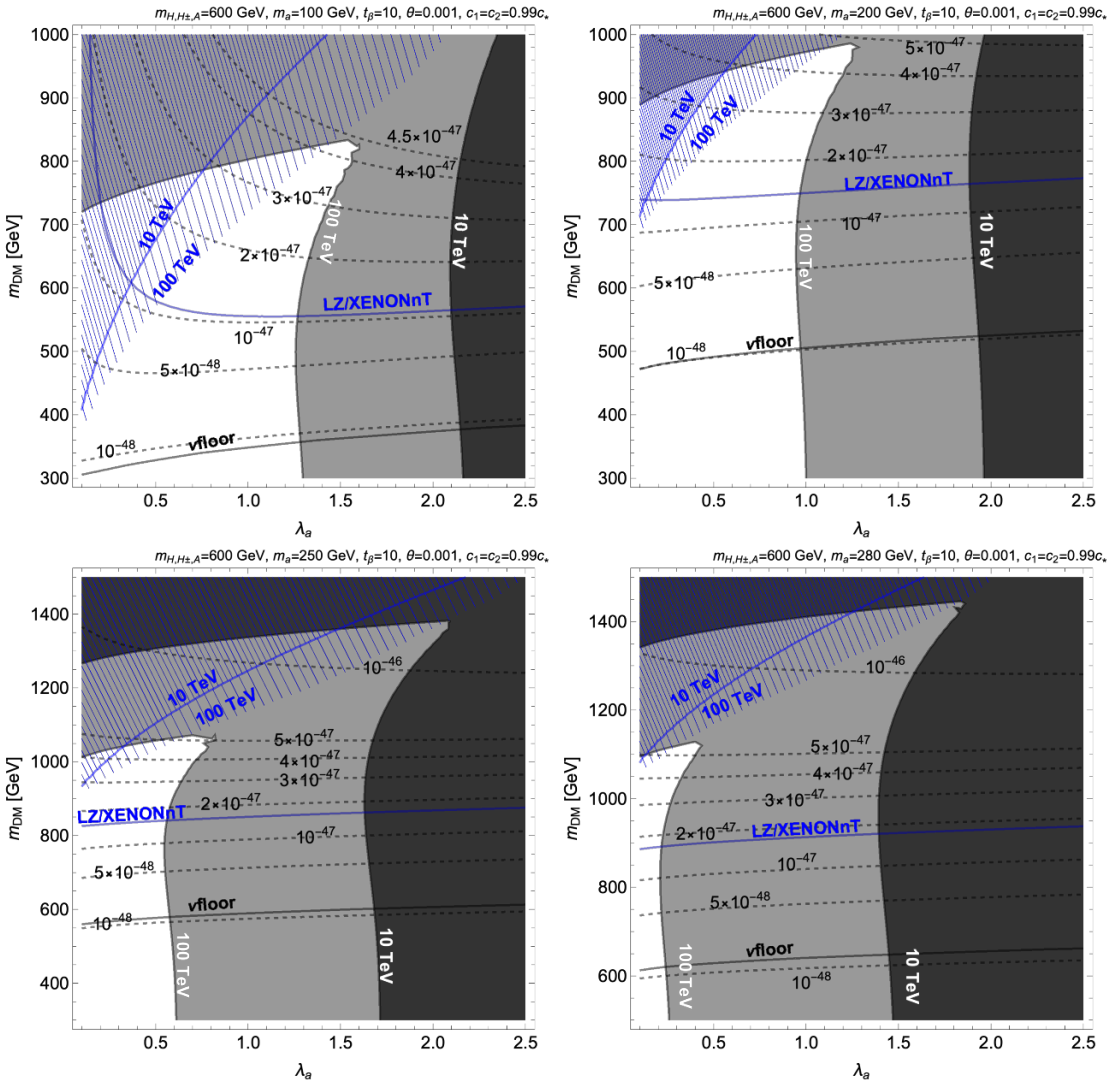

Figure 5. The contours for $\sigma_{\rm SI}$ [cm^2] in λ_a–$m_{\rm DM}$ plane. We take $m_a = 100$, 200, 250, and 280 GeV in each panel. The color notation is the same in figure 3.

is estimated as 100 TeV. Therefore, if the LZ and XENONnT experiments observe the DM signal in future, then this model predicts 600 GeV $\lesssim m_{\rm DM} \lesssim$ 1 TeV.

Acknowledgments

This work was supported by JSPS KAKENHI Grant Number 16K17715, 18H04615 [T.A.] and by Grant-in-Aid for Scientific research from the Ministry of Education, Science, Sports, and Culture (MEXT), Japan, No. 16H06492 [J.H. and Y.S.]. The work of J.H. is also supported by World Premier International Research Center Initiative (WPI Initiative), MEXT, Japan.

JHEP01(2020)114

A Condition for the potential to be bounded below

The potential should be bounded below, namely the potential should be positive for the region where the field values are extremely larger. In this section, we derive the condition for the bounded below.

We focus on the region where the fields take large values, and thus the quadratic and cubic terms in the potential are negligible in the analysis here,

$$V \sim +\frac{1}{2}\lambda_1(H_1^\dagger H_1)^2 + \frac{1}{2}\lambda_2(H_2^\dagger H_2)^2 + \lambda_3(H_1^\dagger H_1)(H_2^\dagger H_2) + \lambda_4(H_1^\dagger H_2)(H_2^\dagger H_1) + \frac{1}{2}\lambda_5\left((H_1^\dagger H_2)^2 + (\text{h.c.})\right) + \frac{\lambda_a}{4}a_0^4 + c_1 a_0^2 H_1^\dagger H_1 + c_2 a_0^2 H_2^\dagger H_2. \tag{A.1}$$

We introduce the following parametrization,

$$H_1^\dagger H_1 = \rho^2 \sin\theta\cos\phi, \tag{A.2}$$

$$H_2^\dagger H_2 = \rho^2 \sin\theta\sin\phi, \tag{A.3}$$

$$H_1^\dagger H_2 = \rho^2 \sin\theta\sqrt{\cos\phi\sin\phi}e^{-i\theta_3}\cos\omega, \tag{A.4}$$

$$a_0^2 = \rho^2\cos\theta, \tag{A.5}$$

where $\rho^2 > 0$, $0 \le \theta \le \pi/2$, and $0 \le \phi \le \pi/2$. Using these parameters, the scalar potential is written as

$$\frac{V}{\rho^4} \sim \tilde{V} \equiv \frac{1}{2}\lambda_1\sin^2\theta\cos^2\phi + \frac{1}{2}\lambda_2\sin^2\theta\sin^2\phi + \frac{1}{2}\left[\lambda_3 + (\lambda_4 + \lambda_5\cos\theta_3)\cos^2\omega\right]\sin^2\theta\sin(2\phi) + \frac{\lambda_a}{4}\cos^2\theta + \frac{1}{2}c_1\sin(2\theta)\cos\phi + \frac{1}{2}c_2\sin(2\theta)\sin\phi. \tag{A.6}$$

By imposing $\tilde{V} > 0$, we find constraints on the parameters.

There is a relation we will use in the rest of this section. Assume $a > 0$, $b > 0$, and $0 < \theta < \pi/2$, then

$$a\cos^2\theta + b\sin^2\theta + 2c\sin\theta\cos\theta > 0 \tag{A.7}$$

if $c + \sqrt{ab} > 0$. The proof is the following.

$$\begin{aligned} a\cos^2\theta + b\sin^2\theta + 2c\sin\theta\cos\theta &= \left(\sqrt{a}\cos\theta \pm \sqrt{b}\sin\theta\right)^2 + 2\sin\theta\cos\theta\left(c \mp \sqrt{ab}\right) \\ &= 2\sin\theta\cos\theta\left(\frac{\left(\sqrt{a}\cos\theta \pm \sqrt{b}\sin\theta\right)^2}{2\sin\theta\cos\theta} + \left(c \mp \sqrt{ab}\right)\right). \end{aligned} \tag{A.8}$$

The sign of the left-hand side is determined by the sign of the terms in the big parenthesis in the right-hand side. It takes minimum if the terms depending on θ vanish, namely, $\sqrt{a}\cos\theta - \sqrt{b}\sin\theta = 0$. Its minimum value is $c + \sqrt{ab}$. Since $\sin\theta\cos\theta > 0$, if $c + \sqrt{ab} > 0$ then the right-hand side is always positive.

JHEP01(2020)114

A.1 $\theta = 0$

For $\theta = 0$, which is the case for $H_1 = H_2 = 0$, we find

$$\tilde{V} = +\frac{\lambda_a}{4}. \tag{A.9}$$

Therefore, $\lambda_a > 0$. This is eq. (3.11).

A.2 $\theta = \pi/2$

For $\theta = \pi/2$, the potential is the same as in the 2HDMs.

$$\tilde{V} = \frac{1}{2}\lambda_1 \cos^2\phi + \frac{1}{2}\lambda_2 \sin^2\phi + \frac{1}{2}\left[\lambda_3 + (\lambda_4 + \lambda_5 \cos\theta_3)\cos^2\omega\right]\sin(2\phi). \tag{A.10}$$

This potential is simplified for $\phi = 0$ and $\pi/2$,

$$\tilde{V} = \begin{cases} \frac{1}{2}\lambda_1 & (\phi = 0) \\ \frac{1}{2}\lambda_2 & (\phi = \pi/2) \end{cases}. \tag{A.11}$$

Therefore, $\lambda_1 > 0$ and $\lambda_2 > 0$ are required. These are eqs. (3.9) and (3.10).

For $\theta = \pi/2$ and $0 < \phi < \pi/2$, the potential is positive if

$$\sqrt{\lambda_1\lambda_2} + \left[\lambda_3 + (\lambda_4 + \lambda_5 \cos\theta_3)\cos^2\omega\right] > 0. \tag{A.12}$$

We can simplify this inequality. If

$$\lambda_4 + \lambda_5 \cos\theta_3 \geq 0, \tag{A.13}$$

then

$$\lambda_3 + (\lambda_4 + \lambda_5 \cos\theta_3)\cos^2\omega \geq \lambda_3, \tag{A.14}$$

and thus

$$\sqrt{\lambda_1\lambda_2} + \left[\lambda_3 + (\lambda_4 + \lambda_5 \cos\theta_3)\cos^2\omega\right] \geq \sqrt{\lambda_1\lambda_2} + \lambda_3. \tag{A.15}$$

If

$$\lambda_4 + \lambda_5 \cos\theta_3 < 0, \tag{A.16}$$

then

$$\lambda_3 + (\lambda_4 + \lambda_5 \cos\theta_3)\cos^2\omega \geq \lambda_3 + (\lambda_4 + \lambda_5 \cos\theta_3) \geq \lambda_3 + (\lambda_4 - |\lambda_5|), \tag{A.17}$$

and thus

$$\sqrt{\lambda_1\lambda_2} + \left[\lambda_3 + (\lambda_4 + \lambda_5 \cos\theta_3)\cos^2\omega\right] \geq \sqrt{\lambda_1\lambda_2} + \left[\lambda_3 + (\lambda_4 - |\lambda_5|)\right]. \tag{A.18}$$

As a result, we can simplify $\sqrt{\lambda_1\lambda_2} + \left[\lambda_3 + (\lambda_4 + \lambda_5 \cos\theta_3)\cos^2\omega\right] > 0$ as

$$\sqrt{\lambda_1\lambda_2} + \lambda_3 + \min\left(0, \lambda_4 - |\lambda_5|\right) > 0. \tag{A.19}$$

This is eqs. (3.12) and the same as a condition given in the 2HDMs with softly broken Z_2 symmetry [32–35].

JHEP01(2020)114

A.3 $\phi = 0$ and $0 < \theta < \pi/2$

For $\phi = 0$ and $0 < \theta < \pi/2$, which is the direction along $H_2 = 0$, we find

$$\tilde{V} = \frac{1}{2}\lambda_1 \sin^2\theta + \frac{\lambda_a}{4}\cos^2\theta + \frac{1}{2}c_1 \sin(2\theta). \tag{A.20}$$

Since $\lambda_1 > 0$ and $\lambda_a > 0$ are already guaranteed, this is positive if

$$c_1 + \sqrt{\frac{\lambda_1 \lambda_a}{2}} > 0. \tag{A.21}$$

This is eqs. (3.13).

A.4 $\phi = \pi/2$ and $0 < \theta < \pi/2$

For $\phi = \pi/2$ and $0 < \theta < \pi/2$, which is the direction along $H_1 = 0$, we find

$$\tilde{V} = +\frac{1}{2}\lambda_2 \sin^2\theta + \frac{\lambda_a}{4}\cos^2\theta + \frac{1}{2}c_2 \sin(2\theta). \tag{A.22}$$

Since $\lambda_2 > 0$ and $\lambda_a > 0$ are already guaranteed, this is positive if

$$c_2 + \sqrt{\frac{\lambda_2 \lambda_a}{2}} > 0. \tag{A.23}$$

This is eqs. (3.14).

A.5 $0 < \phi < \pi/2$ and $0 < \theta < \pi/2$

For $0 < \phi < \pi/2$ and $0 < \theta < \pi/2$, we need some algebra. First of all, we can rewrite $\tilde{V}$ as

$$\begin{aligned}\tilde{V} = &\left(\frac{1}{2}\lambda_1 \cos^2\phi + \frac{1}{2}\lambda_2 \sin^2\phi + \frac{1}{2}\left[\lambda_3 + (\lambda_4 + \lambda_5 \cos\theta_3)\cos^2\omega\right]\sin(2\phi)\right)\sin^2\theta \\ &+ \frac{\lambda_a}{4}\cos^2\theta + (c_1\cos\phi + c_2 \sin\phi)\sin\theta\cos\theta.\end{aligned} \tag{A.24}$$

Since we have already discussed the positivity of $\tilde{V}$ for $\theta = 0$ and $\pi/2$, we can assume the coefficients of $\cos^2\theta$ and $\sin^2\theta$ are positive. Then, $\tilde{V}$ is positive if

$$(c_1\cos\phi + c_2\sin\phi) + \sqrt{\left(\lambda_1\cos^2\phi + \lambda_2\sin^2\phi + \left[\lambda_3 + (\lambda_4 + \lambda_5\cos\theta_3)\cos^2\omega\right]\sin(2\phi)\right)\frac{\lambda_a}{2}} > 0. \tag{A.25}$$

This should be true for all θ_3 and ω. There for, the following inequality should be satisfied,

$$(c_1\cos\phi + c_2\sin\phi) + \sqrt{\left(\lambda_1\cos^2\phi + \lambda_2\sin^2\phi + \tilde{\lambda}_3\sin(2\phi)\right)\frac{\lambda_a}{2}} > 0, \tag{A.26}$$

where

$$\tilde{\lambda}_3 = \lambda_3 + \min(0, \lambda_4 - |\lambda_5|). \tag{A.27}$$

JHEP01(2020)114

Eq. (A.26) is satisfied for $c_1 \cos\phi + c_2 \sin\phi > 0$. Therefore, eq. (A.26) is satisfied for $c_1 \geq 0$ and $c_2 \geq 0$. In the following, we simplify eq. (A.26) for $c_1 < 0$ or $c_2 < 0$.

For $c_1 \cos\phi + c_2 \sin\phi < 0$, we can rewrite eq. (A.26) as

$$\sqrt{\left(\lambda_1 \cos^2\phi + \lambda_2 \sin^2\phi + \tilde{\lambda}_3 \sin(2\phi)\right)\frac{\lambda_a}{2}} > -\left(c_1 \cos\phi + c_2 \sin\phi\right). \tag{A.28}$$

Since the both side are positive, we can square them and find

$$\left(\frac{\lambda_a\lambda_1}{2} - c_1^2\right)\cos^2\phi + \left(\frac{\lambda_a\lambda_2}{2} - c_2^2\right)\sin^2\phi + \left(\frac{\lambda_a\tilde{\lambda}_3}{2} - c_1c_2\right)\sin 2\phi > 0. \tag{A.29}$$

We start from the case for $c_1 > 0$ and $c_2 < 0$. In this case, $c_1 \cos\phi + c_2 \sin\phi < 0$ for $\phi_0 < \phi < \pi/2$, where $\tan\phi_0 = \frac{c_1}{|c_2|}$. It is useful to define

$$f(x) = Ax^2 + B + 2Dx, \tag{A.30}$$

where

$$A = \frac{\lambda_a\lambda_1}{2} - c_1^2, \tag{A.31}$$

$$B = \frac{\lambda_a\lambda_2}{2} - c_2^2, \tag{A.32}$$

$$D = \frac{\lambda_a\tilde{\lambda}_3}{2} - c_1c_2. \tag{A.33}$$

Eq. (A.29) is satisfied if $f(x) > 0$ for $0 < x < \frac{|c_2|}{c_1}$. We find

$$f(0) = \frac{\lambda_a\lambda_2}{2} - c_2^2 = \left(\sqrt{\frac{\lambda_a\lambda_2}{2}} + c_2\right)\left(\sqrt{\frac{\lambda_a\lambda_2}{2}} - c_2\right), \tag{A.34}$$

$$f(\cot\phi_0) = \left(\frac{|c_2|}{c_1}\sqrt{\frac{\lambda_a\lambda_1}{2}} - \sqrt{\frac{\lambda_a\lambda_2}{2}}\right)^2 + \lambda_a\frac{|c_2|}{c_1}\left(\tilde{\lambda}_3 + \sqrt{\lambda_1\lambda_2}\right). \tag{A.35}$$

These two are always positive thanks to $c_2 < 0$, eq. (3.12), and eq. (3.14). Therefore, $f(x) > 0$ at the boundary. It is easy to find that $f(x) > 0$ for $0 < x < \frac{|c_2|}{c_1}$ if one of the following conditions is satisfied,

$$A \leq 0, \tag{A.36}$$

$$\text{or } A > 0 \quad \text{and} \quad -\frac{D}{A} \leq 0, \tag{A.37}$$

$$\text{or } A > 0 \quad \text{and} \quad -\frac{D}{A} \geq \frac{|c_2|}{c_1}, \tag{A.38}$$

$$\text{or } A > 0 \quad \text{and} \quad 0 < -\frac{D}{A} < \frac{|c_2|}{c_1} \quad \text{and} \quad B - \frac{D^2}{A} > 0. \tag{A.39}$$

JHEP01(2020)114

The first condition is that $f(x)$ is convex upward. The second and third conditions are for the $\min(f(x))$ is out of $0 < x < \cot\phi_0$. The last condition is that the minimum exists for $0 < x < \cot\phi_0$ and it is positive. These conditions are simplified as

$$A \leq \frac{c_1}{|c_2|}\sqrt{B}, \tag{A.40}$$

$$\text{or } A < \frac{c_1}{|c_2|}\sqrt{B} \quad \text{and} \quad -\sqrt{AB} < D, \tag{A.41}$$

$$\text{or } A < \frac{c_1}{|c_2|}\sqrt{B} \quad \text{and} \quad D \leq -A\frac{|c_2|}{c_1}. \tag{A.42}$$

After substituting A, B, and D into these conditions, we find that $\tilde{V}$ is positive for $c_1 > 0$ and $c_2 < 0$ if

$$\lambda_1 \leq \lambda_2 \frac{c_1^2}{c_2^2}, \tag{A.43}$$

$$\text{or } \lambda_1 > \lambda_2 \frac{c_1^2}{c_2^2} \quad \text{and} \quad \frac{\lambda_a\tilde{\lambda}_3}{2} - c_1c_2 + \sqrt{\left(\frac{\lambda_a\lambda_1}{2} - c_1^2\right)\left(\frac{\lambda_a\lambda_2}{2} - c_2^2\right)} > 0. \tag{A.44}$$

We find that eq. (A.42) is inconsistent with eq. (3.12).

In a similar manner, we find the conditions for $c_1 < 0$ and $c_2 > 0$ as

$$\lambda_2 \leq \lambda_1 \frac{c_2^2}{c_1^2}, \tag{A.45}$$

$$\text{or } \lambda_2 > \lambda_1 \frac{c_2^2}{c_1^2} \quad \text{and} \quad \frac{\lambda_a\tilde{\lambda}_3}{2} - c_1c_2 + \sqrt{\left(\frac{\lambda_a\lambda_1}{2} - c_1^2\right)\left(\frac{\lambda_a\lambda_2}{2} - c_2^2\right)} > 0. \tag{A.46}$$

For $c_1 < 0$ and $c_2 < 0$, $c_1 = 0$ and $c_2 < 0$, or $c_1 < 0$ and $c_2 = 0$, we find

$$\frac{\lambda_a\tilde{\lambda}_3}{2} - c_1c_2 + \sqrt{\left(\frac{\lambda_a\lambda_1}{2} - c_1^2\right)\left(\frac{\lambda_a\lambda_2}{2} - c_2^2\right)} > 0. \tag{A.47}$$

Eqs. (A.43)–(A.47) are summarized as follows.

$$\begin{cases} \lambda_1 \leq \lambda_2 \frac{c_1^2}{c_2^2}, \\ \lambda_1 > \lambda_1 \frac{c_1^2}{c_2^2} \quad \text{and} \quad \frac{\lambda_a\tilde{\lambda}_3}{2} - c_1c_2 + \sqrt{\left(\frac{\lambda_a\lambda_1}{2} - c_1^2\right)\left(\frac{\lambda_a\lambda_2}{2} - c_2^2\right)} > 0. \end{cases} \qquad (c_1 > 0, c_2 < 0) \tag{A.48}$$

$$\begin{cases} \lambda_2 \leq \lambda_1 \frac{c_2^2}{c_1^2}, \\ \lambda_2 > \lambda_1 \frac{c_2^2}{c_1^2} \quad \text{and} \quad \frac{\lambda_a\tilde{\lambda}_3}{2} - c_1c_2 + \sqrt{\left(\frac{\lambda_a\lambda_1}{2} - c_1^2\right)\left(\frac{\lambda_a\lambda_2}{2} - c_2^2\right)} > 0. \end{cases} \qquad (c_1 < 0, c_2 > 0) \tag{A.49}$$

$$\frac{\lambda_a\tilde{\lambda}_3}{2} - c_1c_2 + \sqrt{\left(\frac{\lambda_a\lambda_1}{2} - c_1^2\right)\left(\frac{\lambda_a\lambda_2}{2} - c_2^2\right)} > 0. \qquad (c_1 \leq 0, c_2 \leq 0). \tag{A.50}$$

JHEP01(2020)114

They can be further simplified as follows.

$$\begin{cases} \sqrt{\lambda_1}c_2 + \sqrt{\lambda_2}c_1 \geq 0, \\ \sqrt{\lambda_1}c_2 + \sqrt{\lambda_2}c_1 < 0 \quad \text{and} \quad \frac{\lambda_a\tilde{\lambda}_3}{2} - c_1c_2 + \sqrt{\left(\frac{\lambda_a\lambda_1}{2} - c_1^2\right)\left(\frac{\lambda_a\lambda_2}{2} - c_2^2\right)} > 0. \end{cases} \tag{A.51}$$

Eq. (A.51) should be satisfied for any c_1 and c_2.

B Beta functions

$$(4\pi)^2\mu\frac{d\lambda_a}{d\mu} = 18\lambda_a^2 - 4g_\chi^4 + 4\lambda_a g_\chi^2 + 8c_1^2 + 8c_2^2, \tag{B.1}$$

$$(4\pi)^2\mu\frac{dc_1}{d\mu} = 8c_1^2 - \frac{3}{2}c_1\left(g_1^2 + 3g_2^2\right) + 2c_1\left(3\lambda_1 + 3\lambda_a + g_\chi^2\right) + 2c_2\left(2\lambda_3 + \lambda_4\right), \tag{B.2}$$

$$(4\pi)^2\mu\frac{dc_2}{d\mu} = 8c_2^2 - \frac{3}{2}c_2\left(g_1^2 + 3g_2^2\right) + 2c_2\left(3\lambda_2 + 3\lambda_a + g_\chi^2 + 3y_t^2\right) + 2c_1\left(2\lambda_3 + \lambda_4\right), \tag{B.3}$$

$$(4\pi)^2\mu\frac{dg_\chi}{d\mu} = 4g_\chi^3. \tag{B.4}$$

References

[1] Planck collaboration, *Planck 2018 results. VI. Cosmological parameters*, arXiv:1807.06209 [INSPIRE].

[2] B.W. Lee and S. Weinberg, *Cosmological Lower Bound on Heavy Neutrino Masses*, *Phys. Rev. Lett.* **39** (1977) 165 [INSPIRE].

[3] XENON collaboration, *Dark Matter Search Results from a One Ton-Year Exposure of XENON1T*, *Phys. Rev. Lett.* **121** (2018) 111302 [arXiv:1805.12562] [INSPIRE].

[4] M. Escudero, A. Berlin, D. Hooper and M.-X. Lin, *Toward (Finally!) Ruling Out Z and Higgs Mediated Dark Matter Models*, *JCAP* **12** (2016) 029 [arXiv:1609.09079] [INSPIRE].

[5] M. Escudero, D. Hooper and S.J. Witte, *Updated Collider and Direct Detection Constraints on Dark Matter Models for the Galactic Center Gamma-Ray Excess*, *JCAP* **02** (2017) 038 [arXiv:1612.06462] [INSPIRE].

[6] S. Ipek, D. McKeen and A.E. Nelson, *A Renormalizable Model for the Galactic Center Gamma Ray Excess from Dark Matter Annihilation*, *Phys. Rev.* **D 90** (2014) 055021 [arXiv:1404.3716] [INSPIRE].

[7] K. Ghorbani, *Fermionic dark matter with pseudo-scalar Yukawa interaction*, *JCAP* **01** (2015) 015 [arXiv:1408.4929] [INSPIRE].

[8] S. Baek, P. Ko and J. Li, *Minimal renormalizable simplified dark matter model with a pseudoscalar mediator*, *Phys. Rev.* **D 95** (2017) 075011 [arXiv:1701.04131] [INSPIRE].

JHEP01(2020)114

[9] C. Gross, O. Lebedev and T. Toma, *Cancellation Mechanism for Dark-Matter-Nucleon Interaction*, *Phys. Rev. Lett.* **119** (2017) 191801 [arXiv:1708.02253] [INSPIRE].

[10] J.M. No, *Looking through the pseudoscalar portal into dark matter: Novel mono-Higgs and mono-Z signatures at the LHC*, *Phys. Rev.* **D 93** (2016) 031701 [arXiv:1509.01110] [INSPIRE].

[11] D. Goncalves, P.A.N. Machado and J.M. No, *Simplified Models for Dark Matter Face their Consistent Completions*, *Phys. Rev.* **D 95** (2017) 055027 [arXiv:1611.04593] [INSPIRE].

[12] M. Bauer, U. Haisch and F. Kahlhoefer, *Simplified dark matter models with two Higgs doublets: I. Pseudoscalar mediators*, *JHEP* **05** (2017) 138 [arXiv:1701.07427] [INSPIRE].

[13] P. Tunney, J.M. No and M. Fairbairn, *Probing the pseudoscalar portal to dark matter via $\bar{b}bZ(\to \ell\ell) + \not{E}_T$: From the LHC to the Galactic Center excess*, *Phys. Rev.* **D 96** (2017) 095020 [arXiv:1705.09670] [INSPIRE].

[14] G. Arcadi, M. Lindner, F.S. Queiroz, W. Rodejohann and S. Vogl, *Pseudoscalar Mediators: A WIMP model at the Neutrino Floor*, *JCAP* **03** (2018) 042 [arXiv:1711.02110] [INSPIRE].

[15] P. Pani and G. Polesello, *Dark matter production in association with a single top-quark at the LHC in a two-Higgs-doublet model with a pseudoscalar mediator*, *Phys. Dark Univ.* **21** (2018) 8 [arXiv:1712.03874] [INSPIRE].

[16] N.F. Bell, G. Busoni and I.W. Sanderson, *Loop Effects in Direct Detection*, *JCAP* **08** (2018) 017 [*Erratum JCAP* **01** (2019) E01] [arXiv:1803.01574] [INSPIRE].

[17] T. Li, *Revisiting the direct detection of dark matter in simplified models*, *Phys. Lett.* **B 782** (2018) 497 [arXiv:1804.02120] [INSPIRE].

[18] LHC Dark Matter Working Group, *LHC Dark Matter Working Group: Next-generation spin-0 dark matter models*, in press [*Phys. Dark Univ.* (2019)] [arXiv:1810.09420] [INSPIRE].

[19] T. Abe, M. Fujiwara and J. Hisano, *Loop corrections to dark matter direct detection in a pseudoscalar mediator dark matter model*, *JHEP* **02** (2019) 028 [arXiv:1810.01039] [INSPIRE].

[20] LUX-ZEPLIN collaboration, *Projected WIMP Sensitivity of the LUX-ZEPLIN (LZ) Dark Matter Experiment*, arXiv:1802.06039 [INSPIRE].

[21] XENON collaboration, *Physics reach of the XENON1T dark matter experiment*, *JCAP* **04** (2016) 027 [arXiv:1512.07501] [INSPIRE].

[22] V.D. Barger, J.L. Hewett and R.J.N. Phillips, *New Constraints on the Charged Higgs Sector in Two Higgs Doublet Models*, *Phys. Rev.* **D 41** (1990) 3421 [INSPIRE].

[23] Y. Grossman, *Phenomenology of models with more than two Higgs doublets*, *Nucl. Phys.* **B 426** (1994) 355 [hep-ph/9401311] [INSPIRE].

[24] M. Aoki, S. Kanemura, K. Tsumura and K. Yagyu, *Models of Yukawa interaction in the two Higgs doublet model and their collider phenomenology*, *Phys. Rev.* **D 80** (2009) 015017 [arXiv:0902.4665] [INSPIRE].

[25] R. Sato, *SimpleBounce: a simple package for the false vacuum decay*, arXiv:1908.10868 [INSPIRE].

[26] A. Drozd, B. Grzadkowski, J.F. Gunion and Y. Jiang, *Extending two-Higgs-doublet models by a singlet scalar field — the Case for Dark Matter*, *JHEP* **11** (2014) 105 [arXiv:1408.2106] [INSPIRE].

JHEP01(2020)114

[27] J. Horejsi and M. Kladiva, *Tree-unitarity bounds for THDM Higgs masses revisited*, *Eur. Phys. J.* **C 46** (2006) 81 [hep-ph/0510154] [INSPIRE].

[28] M. Muhlleitner, M.O.P. Sampaio, R. Santos and J. Wittbrodt, *The N2HDM under Theoretical and Experimental Scrutiny*, *JHEP* **03** (2017) 094 [arXiv:1612.01309] [INSPIRE].

[29] K.G. Klimenko, *On Necessary and Sufficient Conditions for Some Higgs Potentials to Be Bounded From Below*, *Theor. Math. Phys.* **62** (1985) 58 [*Teor. Mat. Fiz.* **62** (1985) 87] [INSPIRE].

[30] P. Bandyopadhyay, E.J. Chun and R. Mandal, *Scalar Dark Matter in Leptophilic Two-Higgs-Doublet Model*, *Phys. Lett.* **B 779** (2018) 201 [arXiv:1709.08581] [INSPIRE].

[31] P. Cushman et al., *Working Group Report: WIMP Dark Matter Direct Detection*, in proceedings of the *Community Summer Study 2013: Snowmass on the Mississippi (CSS2013)*, Minneapolis, MN, U.S.A., 29 July–6 August 2013, arXiv:1310.8327 [INSPIRE]

[32] N.G. Deshpande and E. Ma, *Pattern of Symmetry Breaking with Two Higgs Doublets*, *Phys. Rev.* **D 18** (1978) 2574 [INSPIRE].

[33] M. Sher, *Electroweak Higgs Potentials and Vacuum Stability*, *Phys. Rept.* **179** (1989) 273 [INSPIRE].

[34] S. Nie and M. Sher, *Vacuum stability bounds in the two Higgs doublet model*, *Phys. Lett.* **B 449** (1999) 89 [hep-ph/9811234] [INSPIRE].

[35] S. Kanemura, T. Kasai and Y. Okada, *Mass bounds of the lightest CP even Higgs boson in the two Higgs doublet model*, *Phys. Lett.* **B 471** (1999) 182 [hep-ph/9903289] [INSPIRE].

JHEP01(2020)114